Available online at www.sciencedirect.com
ScienceDirect
Journal of Molecular Graphics and Modelling 25 (2006) 434–441
Journal of Molecular Graphics and Modelling
www.elsevier.com/locate/JMGM

Homology modeling and molecular dynamics study of chorismate synthase from *Shigella flexneri*

Hong Zhou [1], N. Jiten Singh [1], Kwang S. Kim *

Department of Chemistry, Division of Molecular and Life Sciences, Pohang University of Science and Technology, San 31, Hyojadong, Namgu, Pohang 790-784, Republic of Korea

Received 1 October 2005; received in revised form 17 February 2006; accepted 17 February 2006
Available online 17 April 2006

Abstract

Shigellosis is a major public health problem in many developing countries. Antibiotic therapy can reduce the severity of the dysentery and prevent potentially lethal complication. However, owing to the increased resistance to most of the widely used and inexpensive antibiotics, there is an urgent need for new antibacterial agents, particularly those that act on novel targets. Chorismate synthase (CS) is a key enzyme in the shikimic acid pathway, which is essential for the synthesis of aromatic amino acids in bacteria. As an anti-bacterial drug target, CS has been well validated. A homology model of *Shigella*-CS with the flavin mononucleotide (FMN) binding was constructed using the crystal structure of CS from other species. The substrate 5-enolpyruvylshikimate 3-phosphate (EPSP) was subsequently docked into the active site based on previous theoretical studies. Molecular dynamics (MD) was used to refine the starting ternary model. The model was well conserved during the 1.8 ns MD simulation with the equilibrium root mean square deviation (RMSD) value of 3.5 Å. The substrate binding energy was calculated and the electrostatic energy was found to be the most important term for binding. Decomposition of binding energies revealed that R129, R125, R327, R134 and R48 are important residues involved in substrate binding, which is useful for further site-directed mutagenesis experiments. In the absence of crystal structure, our study provides an early insight into the structure of CS from *Shigella flexneri* and its binding to the substrate and cofactor, thus facilitating the inhibitor design.

Keywords: *Shigella flexneri*; Chorismate synthase; Homology modeling; Molecular dynamics simulation; Protein–ligand interaction

1. Introduction

Shigellosis is endemic throughout the world. Worldwide there are ~165 million cases, of which 163 million are in developing countries and 1.5 million in industrialized countries. Each year 1.1 million people are estimated to die from *Shigella* [1]. Effective antimicrobial therapy can reduce the duration and severity of the dysentery and can also prevent potentially lethal complications. However, antimicrobial resistance in enteric pathogens is an ever-growing concern. With the increased resistance to most of the widely used and inexpensive antibiotics (ampicilline, nalidixic acid, cotrimoxazole, tetracycline and chloramphenicol), the effective treatment is becoming increasingly difficult [2,3]. Therefore, there is an urgent need for new antibacterial agents, particularly for those that act on novel targets.

In the seventh i.e., final step of the shikimate biosynthetic pathway, Chorismate synthase (CS) catalyses to convert EPSP to chorismate via a 1,4-trans elimination of phosphate, which leads to the biosynthesis of all aromatic compounds [4]. Because the shikimic acid pathway is absent in humans, it is an attractive target for potential antibiotics. The reaction does not involve a net redox change, but there is an absolute requirement for the reduced FMN as a cofactor [4]. In addition, chorismate lies at a metabolic node, being the precursor for five distinct pathways, and therefore is necessary for the production of folate, *para*-aminobenzoic and other cyclic metabolites such as ubiquinone and menaquinone [5]. CS has long been recognized as a drug target for the antibacterial and antifungal drugs [6]. Until recently, the crystal structure of CS from other species of bacteria has been determined, among which CS from *Streptococcus pneumoniae* (SP) has been cocrystallized with oxidized FMN and EPSP [5]; CS from *Helicobacter pylori*

* Corresponding author. Tel.: +82 54 279 2110; fax: +82 54 279 8137.
E-mail address: kim@postech.ac.kr (K.S. Kim).
[1] These authors contributed equally to this work.

1093-3263/$ – see front matter © 2006 Elsevier Inc. All rights reserved.
doi:10.1016/j.jmgm.2006.02.013

(HP) was determined with the FMN-bound form [7]; CS from another three species are determined in the apo form. No modeling studies on chorismate synthase have been reported so far.

The application of bioinformatics and computational chemistry tools, including sequence/structure database, Modeller, AMBER and CHARMM, etc., has provided an accurate representation of the structure, dynamics, interactions and (free) energetics of a variety of biomolecular systems [8–11]. In our study, we first developed a homology model of the CS from the *Shigella flexneri* (SF) (the predominant species presenting at all times) with the FMN bounding based on the known CS crystal structure using the homology modeling method. After manually docking the EPSP, we performed a 1.8 ns MD simulation to refine the complex structure. Subsequently, the model stability and flexibility were analyzed by RMSD and B-factor plot. In addition, the substrate binding energy was calculated using the Molecular Mechanics/Generalized Born Surface Area (MM-GBSA) method, and the binding energy was decomposed into individual residues that contribute to the substrate binding, which shows the important residues responsible for the substrate binding.

2. Materials and methods

2.1. Material retrieval and sequence alignment

CS from *S. flexneri* (CS-SF) was obtained from the Swiss-Prot-TREMBL database [12]. The templates, the crystal structure of CS from *H. pylori* [7] (CS-HP) (PDB code: 1UM0), from *S. pneumoniae* [5] (CS-SP) (PDB code: 1QXO), from *Saccharomyces cerevisiae* [13] (CS-SC) (PDB code: 1R53), from Aquifex aeolicus [14] (CS-AE) (PDB code: 1Q1L) and from Campylobacter (CS-CA) (PDB code: 1SQ1) were obtained from PDB database [15]. The CS enzyme is a tetramer in all the crystal structures. We extracted the monomer structures and used them as our structure templates. In order to find the proper templates for our homology modeling, we created an identity table between the target sequence and the template sequence (Table 1) [16]. Among the five CS crystal structures, CS-CA, CS-HP and CS-SC share 50.48%, 49.76% and 49.04% sequence identity with our target sequence, respectively, whereas other two crystal structures share low sequence identity with the target. Therefore, we used the first three structures as our templates in the following homology modeling.

Table 1
Sequence identity table of the target sequence with the sequences of the five known crystal structures

	CS-SF	CS-HP	CS-CA	CS-SC	CS-SP	CS-AE
CS-SF	100	49.76	50.48	49.04	33.65	35.34
CS-HP		100	57.93	40.38	31.49	32.93
CS-CA			100	41.35	31.25	31.49
CS-SC				100	30.77	33.41
CS-SP					100	54.81
CS-AE						100

2.2. Model building and evaluation

The 3D model of the CS-SF monomer was built based on three structure templates using Modeller6v2 [17]. The *heteroatom* module in the Modeller6v2 was used to model the CS-SF structure with the FMN binding, which assumes that the ligand interacts similarly with the target and the template. As described above, among five known CS crystal structures, both CS-HP and CS-SP contain FMN. Since CS-HP has a much higher sequence identity with the target sequence, we used the CS-HP-FMN crystal structure as the template for our FMN-binding model building. Multiple structure templates were used to build the CS-HP apo monomer enzyme structure. Subsequently, the model was energetically minimized with 500 steps of steepest decent minimization, followed by 500 steps of conjugate gradient minimization to remove the geometrical strain. To further investigate the EPSP binding with the enzyme, we manually docked the EPSP to the active site based on the previous theoretical study [18] and the substrate binding proposal in CS-PH [7]. This initial ternary complex structure was further refined by the energy minimization and MD simulation. The model structure was evaluated using the Ramachandran plot [19].

2.3. Partial charge calculations

Accurate force fields are essential for reproducing the conformational and dynamic behavior of condensed-phase systems. The AMBER force field is well parameterized for amino acids and nucleic acids. But the parameters for small molecules are still limited for the simulations of more complicated biological systems. In this study, accurate force field parameters for substrate EPSP are thus critical for the computational understanding of enzyme-substrate-cofactor system. Our methods to derive parameters for EPSP are based on the original development of the AMBER03 force field [20], and every effort has been made to maintain the same protocol in creating these new parameters. The substrate EPSP was first extracted from the crystal structure of CS-SP. Then the ligand geometries were optimized using the B3LYP/6-31G* level of theory with the Gaussian 03 suite of programs [21]. Single-point calculations were then performed to obtain the electrostatic potential at the B3LYP/cc-pVTZ level with the polarized continuum model (EPS = 4.0) [20]. Atomic partial charge for the EPSP was computed using the Restrained Electrostatic Potential (RESP) method [22]. The partial charges and the new parameters used here are given as Supplementary material. Parameters for FMN were taken from the work of Schneider and Suhnel [23]

2.4. Molecular dynamics simulation

The AMBER 8.0 program and AMBER 2003 force field were used in our simulation [24]. First, the CS-FMN-EPSP model complex (5579 atoms) was minimized with 500 steps of steepest decent minimization, followed by 500 steps of conjugate gradient minimization to remove the geometrical

strain. The complex was subsequently solvated with the Monte Carlo simulated TIP3P water using the truncated octahedron box extending to 7 Å from the complex [25]. To neutralize the charge of the system, an appropriate number of sodium counterions was added to regions with the largest positive coulombic potentials around the protease. The number of water molecules in the box was 4442 and the box size was ~89 Å × 89 Å × 89 Å.

Subsequently, 1500 steps of minimization were performed on the whole system. This minimized solvated system was used as the starting structure for the following MD simulation. In order to relax the position of water molecules, we performed MD simulation for 20 ps by fixing the solute structure. After that, we performed equilibrium MD simulation for 600 ps at 300 K. We observed that the temperature, pressure, density and total energy of the system were well equilibrated. After this we performed a 1.2 ns production run to assess the time dependent behavior of our molecular system. In all the simulations, bonds involving hydrogen were constrained by applying the shake algorithm [26] to the system, and a time step of 1fs was used.

2.5. Energy calculation

The absolute binding energy of the substrate with the NS3-NS2B was computed using the MM-GBSA methodology [27]. In this approach, an MD simulation is first carried out, and the free energy is calculated from the snapshots taken from the trajectory with counterions and water molecules stripped off, according to Eqs. (1)–(4):

$$G = E_{MM} + G_{sol} - TS \quad (1)$$

$$E_{MM} = E_{es} + E_{vdw} + E_{int} \quad (2)$$

$$G_{sol} = G_{pol\text{-}sol} + G_{nonpol\text{-}sol} \quad (3)$$

$$\Delta G_{bind} = G_{complex} - (G_{receptor} + G_{ligand}) \quad (4)$$

where E_{MM} is the molecular mechanics free energy, G_{sol} the solvation free energy and TS is the product of temperature and entropy. E_{MM} can be divided into contributions from electrostatic (E_{es}), van der Waals (E_{vdw}) and internal (E_{int}) energies. The free energy of solvation G_{sol} uses the generalized Born approach to calculate the electrostatic energy ($G_{pol\text{-}sol}$), coupled with a surface area dependent term for the nonpoloar contribution to solvation ($G_{nonpol\text{-}sol}$). Apart from the calculation of binding affinities of noncovalent associations, MM-GBSA is also applied to decompose the free energies into individual contributions for the in-depth energetic analysis.

In this study, using the last 600 ps of the 1.2 ns production run, the snapshots were collected every 10 ps. Then, MM-GBSA values for each of the total 60 snapshots were averaged to obtain a free energy of association. E_{MM} was calculated with no cutoff for the evaluation of non-bonded interactions. The GB calculation was done by generalized Born methods [28]. The non-polar contribution to the solvation free energy was estimated using Eq. (5):

$$G_{nonpol\text{-}sol} = \gamma SASA \quad (5)$$

where γ represents surface tension and was set to 0.0072 kcal mol^{-1} Å^{-2} and SASA is the solvent-accessible surface area (Å^2) determined using the linear combination of pairwise overlaps (LCPO) model [29] implemented in AMBER. Estimates of conformational entropies were calculated with the nmode module (normal mode analysis) of AMBER8 [24]. In this calculation, we have extracted coordinates for every 50 ps from the trajectory file of the last 600 ps of the MD production run. As the total of number of atoms for CS-FMN-EPSP is more than 5500 atoms, we cut the residues 1–44 (N-terminal residues), 68–84 (includes loop 4), 249–269 (loop 9) and 335–361 (C-terminal residues), thereby the size of the protein system was reduced to four fragments with N-terminal and C-terminal atoms of the fragments appropriately added. The total number of atoms in the CS-FMN-EPSP complex is 3937 atoms.

3. Results and discussion

3.1. Sequence alignment and model building

Recent studies have demonstrated that a sequence identity higher than 25% between two proteins is indicative of similar three-dimensional structures [30]. The high sequence identity between our target and templates shown in Table 1 and Fig. 1 ensure the quality of the homology model. Further energy minimization was performed to remove the geometric restraints before the model CS-SF-FMN was constructed. Fig. 2a shows the superposition of the model of CS-SF-FMN with CS-HP-FMN. As expected, the overall conformation of the model is very similar to the template. Even the amino acids involved in the FMN binding are well conserved as shown in Fig. 2b.

In order to investigate the substrate EPSP binding with the enzyme, we attempted to dock the EPSP to the active site before we performed the MD simulation. According to Ganem's density functional calculations of the mechanism of the anti-1,4-elimination of phosphate from EPSP catalyzed by CS, the energy minimum of the supermolecule formed between FMN-H (FMNH) and *cis*-3,4-dihydroxycyclohexene-1-carboxylic acid-3-phosphate (DHCCP), which lacks the C(5)-enolpyruvate side-chain of EPSP, indicated that the carbocyclic ring of DHCCP is located on the reface of FMN. [18] According to Suh and coworkers' proposal, EPSP is supposed to interact with a number of positively charged residues since it is highly negatively charged [7], and the EPSP binding mode was proposed. Based on these studies, we extract the EPSP from the crystal structure of CS-SP and dock it to the reface of FMN in the model active site, manually adjusting the amino acid side chain in the active site for the salt bridge interactions with EPSP. Fig. 3a shows our model of CS-SF-FMN-EPSP after manual docking, followed by energy minimization. A Ramachandran plot of this minimized model complex showed that 95.3% backbone angles are in the allowed region,

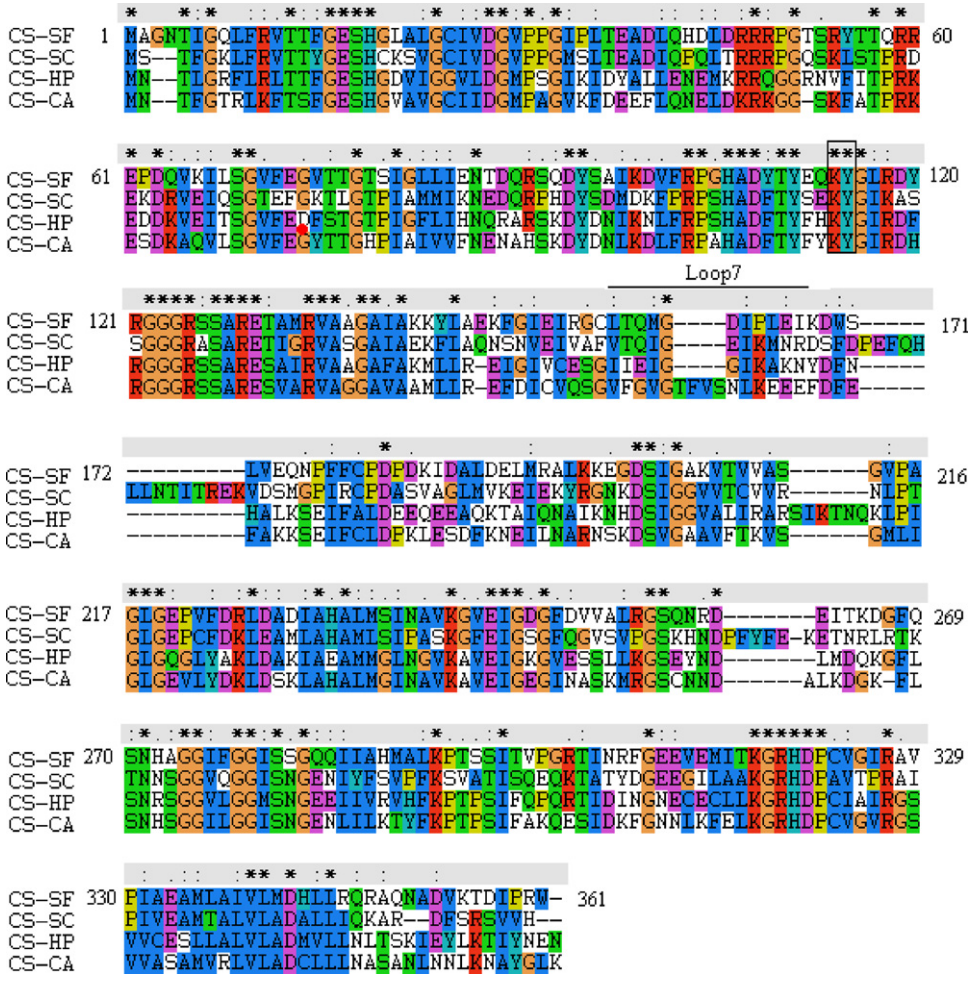

Fig. 1. Multiple sequence alignment between the target sequence and the three template sequences. Stars and dots above the alignment show the residues that are identical or highly homologous, respectively.

indicating that our initial model can be safely used in the following MD simulation.

3.2. MD simulations

To explore the intrinsic dynamics and the structural stability of our ternary model, we performed the 1.8 ns MD simulation without any harmonic restraints on the model. To evaluate the overall stability of our model, we calculated the RMSD from the starting structure for all backbone C alpha atoms as a function of simulation time, as shown in Fig. 4. Stepwise rising of the RMSD correlates well with the equilibrium MD simulation. A plateau of ~3.5 Å RMSD was achieved within 600 ps of unrestrained simulation, suggesting that a 1.8 ns unrestrained simulation was sufficient for stabilizing a fully relaxed model. In order to achieve a more accurate model structure, we calculated the average structure using 600 snapshots of the last 600 ps simulation. A Ramachandran plot of this average structure showed that 97.8% backbone angles are in the allowed region, which signals that the MD simulation further refines the model structure to be more chemically realistic.

The superposition of the averaged structure with the initial minimized structure (Fig. 3b) does not show major conformational change from the initial model, which is consistent with the relatively low RMSD value (Fig. 4). Fig. 3c shows EPSP, FMN and the surrounding amino acid from the active site of the average structure, in which the strong salt bridge interactions of the EPSP carboxyl group with R48, R129, R125, R134 and R327 are observed. When the ring moieties of the average geometry of FMN/EPSP are overlapped with those of the crystal structure, the side chains deviate somewhat from the original crystal structure due to different mode of interaction with the neighboring residues around FMN and EPSP in the CS-FMN-EPSP complex model system (see Supplementary material).

The flexibility of the proteins was assessed by the B-factor from the MD trajectory which reflects the flexibility of each atom in a molecule (Fig. 5a). In a typical B-factor pattern, a low B-factor value indicates the well-structured regions while the high values indicate the loosely structured loop regions or domain terminals [31]. Loops 1–10 in Fig. 5a shows the 10 high B-factor regions, which correspond to the red colored region in Fig. 5b. It is obvious that the major backbone fluctuations occur in the loop region and in the region surrounding the beta–alpha–beta fold, whereas regions with the low B-factor correspond exclusively to the rigid beta–alpha–beta fold. These facts indicate the stability of our model structure.

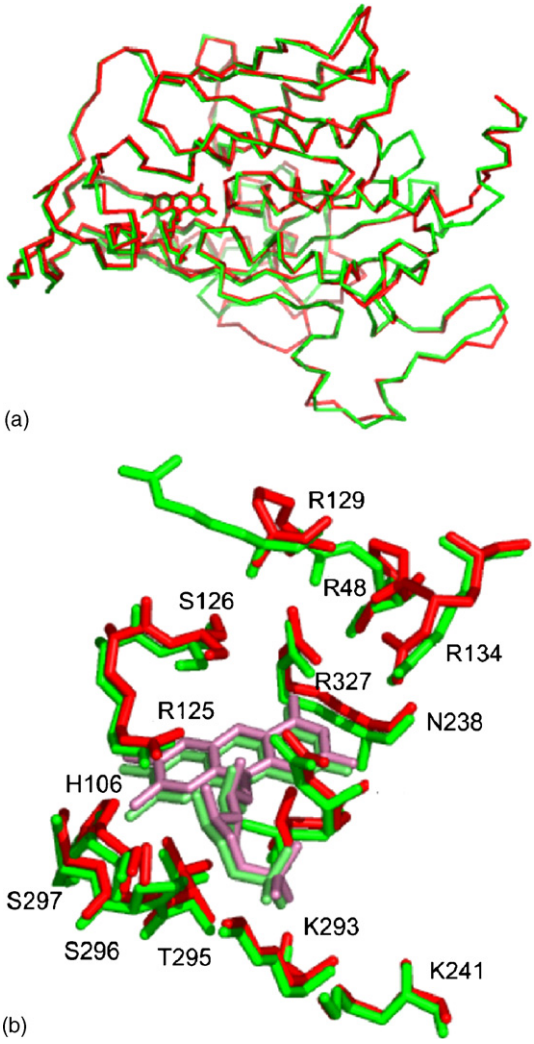

Fig. 2. Model of CS-SF-FMN: (a) superposition of the model structure and the template structure. The crystal structure CS-HP-FMN is colored green; model CS-SF-FMN is colored red. (b) Superposition of the conserved amino acid involved in FMN binding between model and template. The FMN and amino acids from CS-HP are colored green, while those from CS-SF are colored red.

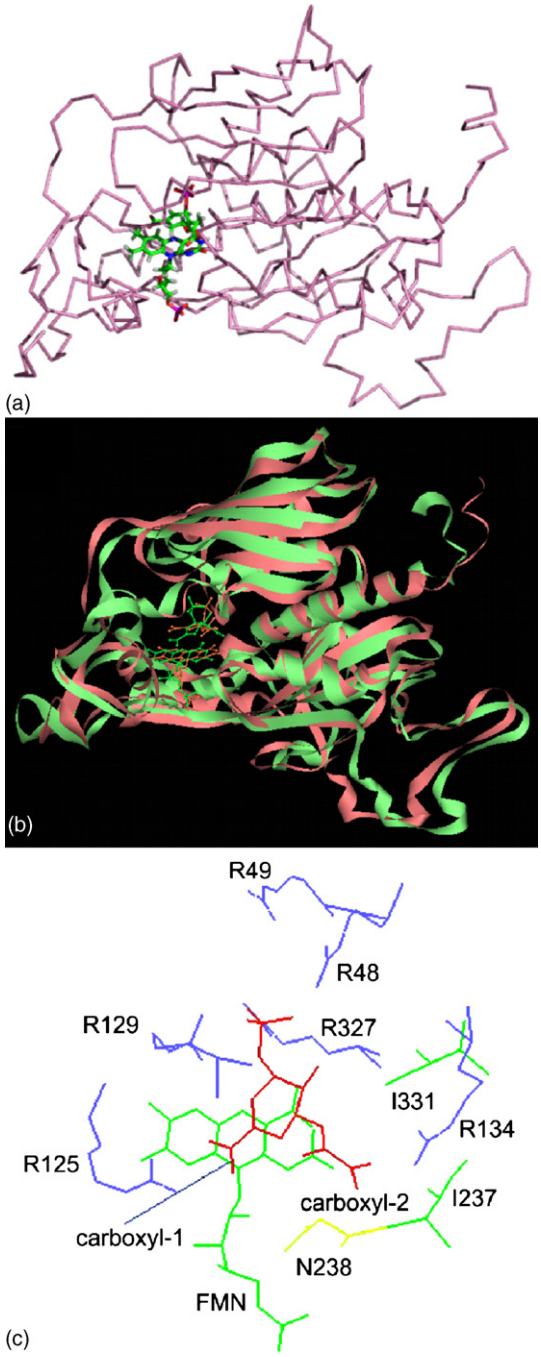

Fig. 3. Model of CS-SF-FMN-EPSP: (a) the model structure of CS-SF-FMN-EPSP after docking EPSP into FMN reface, followed by energy minimization. (b) Superposition of the average structure during the last 600 snapshots with the initial minimized structure. The averaged structure is colored red; the initial structure is colored green. (c) Amino acids involved in EPSP binding from the averaged structure. FMN and EPSP are colored green and red, respectively.

However, two regions with high B-factor values are of alpha helix. 114K and 115Y in Loop6 are two residues showing in the alpha helix region with high B-factor values. We observed that the side chain of these two amino acids intrudes into the interface of the inter-monomers. In addition, the hydrogen bond [32] of backbone 115Y-C═O in chain A and 30S–OH in chain C was found in the CS-HP crystal structure, and the 114K and 115Y are conserved in all sequences, as shown in the black rectangle in Fig. 1. These observations suggest that 114K and 115Y may play important roles in inter-monomer interactions. When only one chain is in simulation, 114K and 115Y lose the interaction with other monomers. As a result, this part will fluctuate significantly to rearrange for its preferred conformation. Another region with a high B-factor value in alpha helix conformation is Loop7 (Fig. 5). This observation may be due to their poor sequence alignment with the template, as shown in Fig. 1.

Finally, from the superposition of the backbone of average structure and initial structure, we observed that the loop region around FMN and EPSP does not change much for the EPSP binding, except for residues 124–126, whose backbone moves backwards slightly for EPSP binding.

Ideally, one would hope to run the tetramer CS MD simulation to better understand the inter-monomer dynamics within the enzyme. This exercise, however, would be expensive in terms of computing cost. Our major goal of this study is to characterize the cofactor and substrate binding mode with the

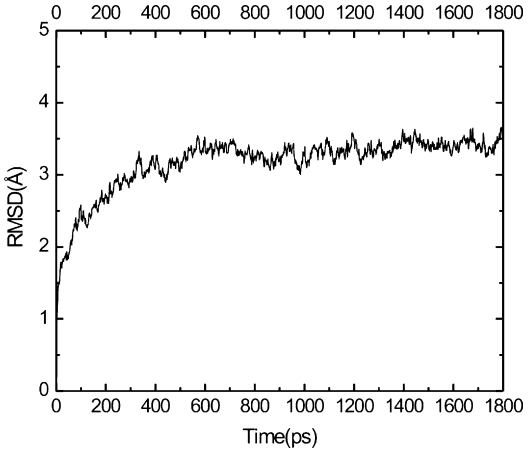

Fig. 4. RMSD of model backbone atoms during 1.8 ns MD simulation.

enzyme, thus helping design a selective anti-*Shigella* drug. Therefore, the simulation of the monomer rather than the tetramer will not change our major conclusions of our study.

3.3. Energy components and residue contributions

The EPSP binding energy with enzyme was calculated from the single trajectory of the complex. The binding energy

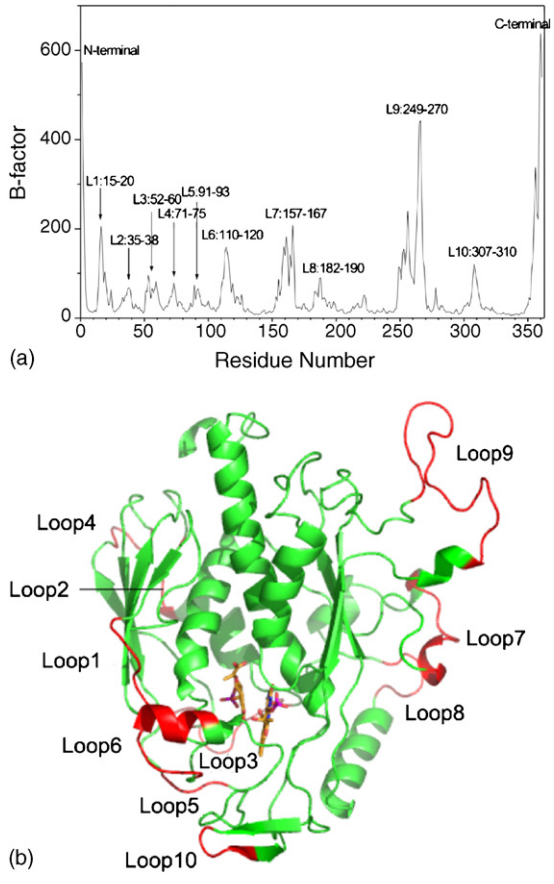

Fig. 5. Model flexibility. (a) Residue fluctuations plotted as B-factors during the 1.8 ns MD simulation. The region with high fluctuation in the simulation is labeled as loops 1–10. (b) The average structure of last 600 snapshots. The regions colored red correspond to the loops 1–10 shown in (a).

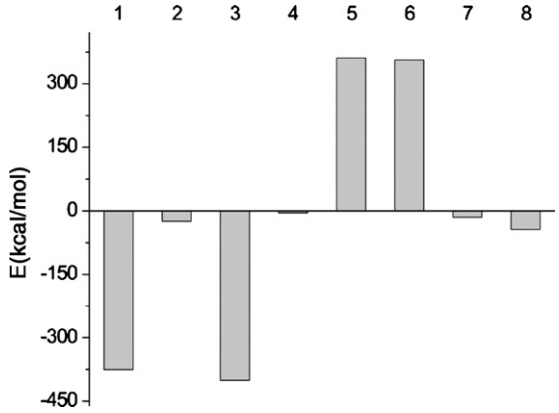

Fig. 6. Energy components (kcal/mol) for the EPSP binding to CS-FMN complex. Components are as follows: (1) electrostatic, (2) van der Waals, (3) molecular mechanics, (4) non-polar solvation, (5) polar solvation, (6) solvation energy, (7) electrostatic + polar solvation, (8) molecular mechanics + solvation energy.

corresponding to the enthalpic contributions to the free energy of binding plus the solvation energy term is 44 ± 5 kcal/mol. The entropic contribution to the binding energy is -17 ± 7.5 kcal/mol. Here the standard deviation is relatively larger as we have considered the fragments of the protein due the large size of the CS-FMN-EPSP complex. With this entropy correction, the binding free energy is 27 kcal/mol. To obtain a detailed picture of the various forces acting in the binding, the binding energy was separated into internal, electrostatic, van der Waals, polar solvation and non-polar solvation (Fig. 6). We found the major contributions to EPSP binding come from electrostatic and van der Waals terms. The nonpolar solvation term contribute slightly for the binding, whereas the polar solvation term opposes the binding.

Furthermore, the binding energy was decomposed into key residues that contribute to the substrate binding (Table 2). Table 2 shows that the salt bridge interactions play an important role in the EPSP binding. Van der Waals contributions to the substrate binding mainly comes from FMN. We also observed that R48 (8 kcal/mol), R125 (12 kal/mol), R129 (13 kcal/mol), R134 (10 kcal/mol) and R327 (10 kcal/mol) are the most

Table 2
Binding free energy is decomposed into major individual residues

Residue	TOT	VDW	ELE	GAS	GBSOL
R129	13.24	0.21	117.79	117.99	104.76
R125	11.98	−0.94	99.93	98.99	87.01
R327	10.07	−0.14	106.41	106.28	96.21
R134	10	−0.63	105.84	105.21	95.21
R48	8.28	0.15	101.73	101.88	93.6
N238	4.71	1.57	11.01	12.58	7.86
FMN	4.35	4.16	−104.93	−100.77	105.12
I237	3.86	0.74	9.31	10.05	6.19
R49	3.73	0.55	86.74	87.29	83.56
I331	1.27	1.01	2.59	3.6	2.33

VDW, ELE and GBSOL stands for Van der Waals energy, electrostatic energy and generalized Born model solvation free energy, respectively; GAS = VDW + ELE, and TOT = GAS + GBSOL. Only the cases where $|TOT| > 1$ kcal/mol are listed in the order of descending of binding energy.

Table 3
Hydrogen bond analysis for the interaction of FMN/EPSP with the different residues of the protein and among themselves during last 600 ps simulation

Electron pair donor	Electron pair acceptor	H-bond occupancy (%)
EPS O3	Arg129 NH_2-HH22	96.33
EPS O5	Thr131 OG1-HG1	74.00
EPS O91	Asn238 N–H	87.17
FMN O4′	ALA107 N–H	84.67
FMN O3′	Ser296 OG-HG	95.83
EPS O11	FMN O2′-HO_2	99.83

H-bond distance cutoff between donor and acceptor and the angle cutoff is 3.5 Å and 120°, respectively.

important residues to anchor EPSP and the binding energy are mainly contributed by salt bridge interactions. This result agrees well with the active site conformation from the average structure (Fig. 3). R129, R48 and R327 interact with the EPSP phosphorus acid group in three different ways. R125 interacts with the EPSP carboxyl group1 and R134 interacts with the EPSP carboxyl group2. For N238, I237, R49 and I331 (Table 2), the binding energy with EPSP comes from both electrostatic energy and the van der Waals energy, but the contributions of the electrostatic energy are much higher than that of the van der Waals energy. Fig. 3 shows the conformations of all these residues and their interaction modes with EPSP. The binding energy analysis suggests the important residues which contribute to the substrate binding.

3.4. Hydrogen bonding interaction with the substrate and cofactor

Enzyme-substrate and enzyme-cofactor hydrogen bonds were analyzed using the PTRAJ module of AMBER8 [24]. We calculated the hydrogen bonds occupancy for the last 600 ps of the MD trajectories (Table 3). The criteria for identifying hydrogen bonds were as follows: (1) the distance between electron donor (X) and electron acceptor (Y) atom was less than or equal to 3.5 Å, (2) the angle Y–H–X was greater than or equal to 120°. Important H-bond interactions are shown in Table 3. We found that both the substrate and the cofactor have stable hydrogen bonds with the surrounding residues. Special attention was given to stable hydrogen bonds, those that persisted throughout for ∼75% or more of the analyzed period.

4. Conclusions

In this study, a 3D structure of the chorismate synthase from *S. flexneri* was investigated with the cofactor (FMN) and substrate (EPSP) binding, based on homology modeling principles and previous theoretical studies. A 1.8 ns MD simulation was performed, with the RMSD value of 3.5 Å at equilibrium. The average structure from the last 600 snapshots of the 1.8 ps simulation was calculated, which did not show major conformational changes compared with the initial minimized model complex. This result agrees with the low RMSD value. The B-factor plot further proves the stability of our model: the flexible region during the simulation corresponds exclusively to the loop region or the regions around the rigid beta–alpha–beta fold of the enzyme. The binding energy calculation showed that van der Waals and electrostatic terms are favorable for the binding, whereas polar solvation opposes the binding. The binding energy decomposition revealed that the R129, R125, R327, R134 and R48 play important roles in substrate binding, which may guide the further site-directed mutagenesis studies. Finally, hydrogen bonds analysis identified the important hydrogen bonds between enzyme and substrate/cofactor.

Acknowledgements

This work was made possible by grants from KOSEF/CRI and BK21.

Appendix A. Supplementary data

Supplementary data associated with this article can be found, in the online version, at doi:10.1016/j.jmgm.2006.02.013.

References

[1] WHO/IVR State of the art of new vaccines, Research & Development, Initiative for Vaccine Research, World Health Organization, Geneva, April 2003, p. 74.
[2] K.L. Kottlof, J.P. Winickoff, B. Ivanoff, Global burden of *Shigella* infections: implications for vaccine development and implementation of control strategies, Bull. World Health Org. 77 (1999) 651–666.
[3] D.A. Sack, C. Lyke, C. McLaughlin, Antimicrobial resistancein shigellosis, cholera and campylobacteriosis. World Health Organization/CDS/DRS/2001.8.
[4] P. Macheroux, J. Schmid, N. Amrhein, A. Schaller, A unique reaction in a common pathway: mechanism and function of chorismate synthase in the shikimate pathway, Planta 207 (1999) 325–334.
[5] J. Maclean, S. Ali, The structure of chorismate synthase reveals a novel flavin binding site fundamental to a unique chemical reaction, Structure 11 (2003) 1499–1511.
[6] E. Haslam, Shikimic Acid: Metabolism and Metabolites, John Wiley & Sons, Chichester, UK, 1993.
[7] H.J. Ahn, H.J. Yoon, B. Lee II, S.W. Suh, Crystal structure of chorismate synthase: a novel FMN-binding protein fold and functional insights, J. Mol. Biol. 336 (2004) 903–915.
[8] T.E. Cheatham III, Simulation and modeling of nucleic acid structure, dynamics and interactions, Curr. Opin. Struct. Biol. 14 (2004) 360–367.
[9] H. Yang, J.H. Ahn, R.K. Ibrahim, S. Lee, Y. Lim, The three-dimensional structure of Arabidopsis thaliana *O*-methyltransferase predicted by homology-based modeling, J. Mol. Graph. Model 23 (2004) 77–87.
[10] A. Marabotti, S. D'Auria, M. Rossi, A.M. Facchiano, Theoretical model of the three-dimensional structure of a sugar binding protein from *Pyrococcus horikoshii*: structural analysis and sugar binding simulations, Biochem. J. 380 (2004) 677–684.
[11] Y. Peng, S.M. Keenan, W.J. Welsh, Structural model of the Plasmodium CDK, Pfmrk, a novel target for malaria therapeutics, J. Mol. Graph. Model 24 (2005) 72–80.
[12] E. Gasteiger, A. Gattiker, C. Hoogland, I. Ivanyi, R.D. Appel, A. Bairoch, ExPASy: The proteomics server for in-depth protein knowledge and analysis, Nucleic Acids Res. 31 (2003) 3784–3788. http://kr.expasy.org/.
[13] S. Quevillon-Cheruel, N. Leulliot, P. Meyer, M. Graille, M. Bremang, K. Blondeau, I. Sorel, A. Poupon, J. Janin, H. van Tilbeurgh, Crystal structure of the bifunctional chorismate synthase from *Saccharomyces cerevisiae*, J Biol. Chem. 279 (2004) 619–625.

[14] C.M. Viola, V. Saridakis, D. Christendat, Crystal structure of chorismate synthase from Aquifex aeolicus reveals a novel beta alpha beta sandwich topology, Proteins 54 (2004) 166–169.
[15] H.M. Berman, J. Westbrook, Z. Feng, G. Gilliland, T.N. Bhat, H. Weissig, I.N. Shindyalov, P.E. Bourne, The protein data bank, Nucleic Acids Res. 28 (2000) 235–242.
[16] W.R. Taylor, Protein residue colour references, Protein Eng. 10 (1997) 743–746. Online: http://emboss.sourceforge.net/Jemboss/jae.html.
[17] A. Sali, T.L. Blundell, Comparative protein modelling by satisfaction of spatial restraints, J. Mol. Biol. 234 (1993) 779–815.
[18] O. Dmitrenko, H.B. Wood, R.D. Bach, B. Ganem, A theoretical study of the chorismate synthase reaction, Org. Lett. 3 (2001) 4137–4140.
[19] N. Guex, M.C. Peitsch, SWISS-MODEL and the Swiss-PdbViewer: an environment for comparative protein modeling, Electrophoresis 18 (1997) 2714–2723.
[20] Y. Duan, C. Wu, S. Chowdhury, M.C. Lee, G. Xiong, W. Zhang, R. Yang, P. Cieplak, R. Luo, T. Lee, J. Caldwell, J. Wang, P. Kollman, A point-charge force field for molecular mechanics simulations of proteins based on condensed-phase quantum mechanical calculations, J. Comput. Chem. 24 (2003) 1999–2012.
[21] M.J. Frisch, G.W. Trucks, H.B. Schlegel, G.E. Scuseria, M.A. Robb, J.R. Cheeseman, J.A. Montgomery Jr., T. Vreven, K.N. Kudin, J.C. Burant, J.M. Millam, S.S. Iyengar, J. Tomasi, V. Barone, B. Mennucci, M. Cossi, G. Scalmani, N. Rega, G.A. Petersson, H. Nakatsuji, M. Hada, M. Ehara, K. Toyota, R. Fukuda, J. Hasegawa, M. Ishida, T. Nakajima, Y. Honda, O. Kitao, H. Nakai, M. Klene, X. Li, J.E. Knox, H.P. Hratchian, J.B. Cross, V. Bakken, C. Adamo, J. Jaramillo, R. Gomperts, R.E. Stratmann, O. Yazyev, A.J. Austin, R. Cammi, C. Pomelli, J.W. Ochterski, P.Y. Ayala, K. Morokuma, G.A. Voth, P. Salvador, J.J. Dannenberg, V.G. Zakrzewski, S. Dapprich, A.D. Daniels, M.C. Strain, O. Farkas, D.K. Malick, A.D. Rabuck, K. Raghavachari, J.B. Foresman, J.V. Ortiz, Q. Cui, A.G. Baboul, S. Clifford, J. Cioslowski, B.B. Stefanov, G. Liu, A. Liashenko, P. Piskorz, I. Komaromi, R.L. Martin, D.J. Fox, T. Keith, M.A. Al-Laham, C.Y. Peng, A. Nanayakkara, M. Challacombe, P.M.W. Gill, B. Johnson, W. Chen, M.W. Wong, C. Gonzalez, J.A. Pople, Gaussian 03, Gaussian, Inc., Wallingford, CT, 2004.
[22] C.I. Bayly, P. Cieplak, W.D. Cornell, P.A. Kollman, A well-behaved electrostatic potential based method using charge restraints for determining atom-centered charges: the RESP model, J. Phys. Chem. 97 (1993) 10269.
[23] C. Schneider, J. Suhnel, A molecular dynamics simulation of the flavin mononucleotide-RNA aptamer complex, Biopolymers 50 (1999) 287–302.
[24] D.A. Case, T.A. Darden, T.E. Cheatham III, C.L. Simmerling, J. Wang, R.E. Duke, R. Luo, K.M. Merz, B. Wang, D.A. Pearlman, M. Crowley, S. Brozell, V. Tsui, H. Gohlke, J. Mongan, V. Hornak, G. Cui, P. Beroza, C. Schafmeister, J.W. Caldwell, W.S. Ross, P.A. Kollman, AMBER8 University of California, San Francisco, 2004.
[25] W.L. Jorgensen, J. Chandrasekhar, J.D. Madura, R.W. Impey, M.L. Klein, Comparison of simple potential functions for simulating liquid water, J. Chem. Phys. 79 (1983) 926–935.
[26] J.-P. Ryckaert, G. Ciccotti, H.J.C. Berendsen, Numerical integration of the Cartesian equations of motion of a system with constraints: Molecular dynamics of *n*-alkanes, J. Comput. Phys. 23 (1977) 327–341.
[27] I. Massova, P.A. Kollman, Combined molecular mechanical and continuum solvent approach (MM-PBSA/GBSA) to predict ligand binding, Perspect. Drug Discov. 18 (2000) 113–135.
[28] V. Tsui, D.A. Case, Theory and applications of the generalized Born solvation model in macromolecular simulations, Biopolymers 56 (2001) 275–291.
[29] J. Weiser, P.S. Shenkin, W.C. Still, Approximate atomic surfaces from linear combinations of pairwise overlaps (LCPO), J. Comput. Chem. 20 (1999) 217–230.
[30] A.S. Yang, B. Honig, An integrated approach to the analysis and modeling of protein sequences and structures, J. Mol. Biol. 301 (2000) 665–711.
[31] C.S. Alexander, X. Yan, T. Pei, Homology modeling and molecular dynamics simulations of transmembrane domain structure of human neuronal nicotinic acetylcholine receptor, Biophys. J. 88 (2005) 1009–1017.
[32] C. Pak, H.M. Lee, J.C. Kim, D. Kim, K.S. Kim, Theoretical investigation of normal to strong hydrogen bonds, Struct. Chem. 16 (2005) 187–202.